J. Plasma Phys. (2021), *vol*. 87, 905870602
Published by Cambridge University Press
doi:10.1017/S0022377821000982

Plasma scale length and quantum electrodynamics effects on particle acceleration at extreme laser plasmas

Ozgur Culfa [1],† **and Sinan Sagir** [2]

[1]Department of Physics, Karamanoglu Mehmetbey University, Karaman 70200, Turkey

[2]Vocational School of Health Services, Karamanoglu Mehmetbey University, Karaman, 70200, Turkey

(Received 5 July 2021; revised 22 September 2021; accepted 23 September 2021)

In this work, simulations of multipetawatt lasers at irradiances $\sim 10^{23}$ W cm^{-2}, striking solid targets and implementing two-dimensional particle-in-cell code was used to study particle acceleration. Preformed plasma at the front surface of a solid target increases both the efficiency of particle acceleration and the reached maximum energy by the accelerated charged particles via nonlinear plasma processes. Here, we have investigated the preformed plasma scale length effects on particle acceleration in the presence and absence of nonlinear quantum electrodynamic (QED) effects, including quantum radiation reaction and multiphoton Breit–Wheeler pair production, which become important at irradiances $\sim 10^{23}$ W cm^{-2}. Our results show that QED effects help particles gain higher energies with the presence of preformed plasma. In the results for all cases, preplasma leads to more efficient laser absorption and produces more energetic charged particles, as expected. In the case where QED is included, however, physical mechanisms changed and generated secondary particles (γ-rays and positrons) reversing this trend. That is, the hot electrons cool down due to QED effects, while ions gain more energy due to different acceleration methods. It is found that more energetic γ-rays and positrons are created with increasing scale length due to high laser conversion efficiency ($\sim$24 % for γ-rays and $\sim$4 % for positrons at $L = 7$ μm scale length), which affects the ion and electron acceleration mechanisms. It is also observed that the QED effect reduces the collimation of angular distribution of accelerated ions because the dominant ion acceleration mechanism is changing when QED is involved in the process.

Key words: PIC simulations, particle acceleration, laser-plasma interactions

1. Introduction

The strong electromagnetic fields in the focus of high-intensity laser pulses ionize matter to produce a plasma in a very short time. Charged particles can be accelerated to very high energies in short distances by the electromagnetic fields generated in this plasma (Daido, Nishiuchi & Pirozhkov 2012; Macchi, Borghesi & Passoni 2013). Therefore, laser–plasma interactions have many potential applications varying from hadron therapy (Bulanov *et al.* 2014) and radiation generation for femtosecond time scale imaging (Blaga *et al.* 2011), to next-generation particle accelerators (if they can be staged) (Tajima & Dawson 1979;

† Email address for correspondence: ozgurculfa@kmu.edu.tr

Esarey, Schroeder & Leemans 2009; Steinke *et al.* 2016). Recent theoretical studies with high intensity laser–solid interactions ($>10^{20}$ W cm^{-2}) show that monoenergetic ions can be accelerated to GeV energy levels (Xu *et al.* 2018), and by altering the target, maximum ion energies can be increased (Sadighi-Bonabi *et al.* 2010; Yazdani *et al.* 2014). At the extreme intensities reaching laser irradiances $>10^{22}$ W cm^{-2}, the solid target is ionized rapidly and the electrons in the generated plasma are accelerated to such ultrarelativistic energies that the electric field they experience in their rest frame may reach the critical or Schwinger field of quantum electrodynamics (QED), $E_s = 1.3 \times 10^{18}$ V m^{-1} (Schwinger 1951). This field is the threshold where QED effects start to become important (Bell & Kirk 2008; Kirk, Bell & Arka 2009). The radiation-dominant regime starts at $a_0 \simeq 400$ where a_0 is the dimensionless laser amplitude given by

$$a_0 = \sqrt{\frac{I_{\mathrm{W\ cm^{-2}}} \lambda^2_{\mu\mathrm{m}}}{1.37 \times 10^{18}}}, \tag{1.1}$$

where I is the intensity (in W cm^{-2}) and λ (in microns) is the wavelength of the incident laser. Furthermore, quantum physics effects begin to present at $a_0 \simeq 2500$ ($I \simeq 1.38 \times 10^{26}$ W cm^{-2}). When $a_0 = 5 \times 10^5$ and $I \simeq 3 \times 10^{29}$ W cm^{-2}, the laser pulse electric field becomes equal to the Schwinger electric field $E_s = m_e^2 c^3 / e\hbar$ and nonlinear QED effects are present, creating electron–positron pairs in the vacuum (Mourou, Tajima & Bulanov 2006).

The development of multipetawatt class lasers (up to 100 PW) mean that intensities of $\sim 10^{23}$ W cm^{-2} will be achievable (Piazza, Muller & Hatsagortsyan 2012; Danson *et al.* 2019), raising a new regime in physics which includes the ion acceleration to GeV energies by the radiation pressure of the laser (Shen *et al.* 2007; Zhang *et al.* 2010; Qiao *et al.* 2012) and the onset of nonlinear QED effects. In this paper, the acceleration of protons, fast electrons, positrons and photons in extreme laser irradiances ($>10^{23}$ W cm^{-2}) have been studied in the presence of QED effects and defined preformed plasma scale lengths.

Particle acceleration with high irradiance laser plasma interactions has been extensively investigated with current PW-class lasers (up to $\sim 10^{21}$ W cm^{-2}) (Wilks *et al.* 2001; McKenna *et al.* 2008; Culfa *et al.* 2016, 2017). Hot electrons can reach GeV energies when interacting with gas targets (Leemans *et al.* 2006; Kneip *et al.* 2009) and 150 MeV with solid targets (Culfa *et al.* 2014, 2016, 2017). Moreover, these generated electrons also lead to the acceleration of protons inside the plasma via several mechanisms (Wilks *et al.* 2001; Albright *et al.* 2007; Yin *et al.* 2007; Jung *et al.* 2013). It is well known that laser absorption and electron acceleration mechanisms have a strong dependence on preformed plasma scale length L and electron number density n_e given by

$$n_e = \frac{\omega_p^2 m_e \epsilon_0}{e^2} \tag{1.2}$$

where ω_p is the plasma frequency, m_e and e is the electron mass and charge, respectively.

Recent simulations with different foil thicknesses between 0.1 and 0.9 μm showed that a 110 nm preformed plasma scale length is optimum for proton acceleration at the relatively lower intensities ($\sim 10^{22}$ W cm^{-2}) possible with 10 PW laser systems (Hadjisolomou *et al.* 2020). For thicker targets with foil thicknesses of a few μm, it is seen that the optimum preformed plasma scale length is around 8 μm for proton acceleration with similar laser intensities ($\sim 10^{21}$–10^{22} W cm^{-2}) (Esirkepov *et al.* 2014). The interaction of a laser pulse with an overdense plasma ($n_e > n_c$), depends on the plasma scale length L. When the scale length is much larger than the electron quiver radius, $r = eE/m\omega^2 \ll L$,

https://doi.org/10.1017/S0022377821000982 Published online by Cambridge University Press

the main laser absorption mechanism is due to nonlinear processes in the plasma resonance region where $n_e \simeq n_c$. Varying density scale length enables an optimum absorption by the resonance absorption mechanism (Kruer 1988). For the case of $L \gg r$, the mechanism of electron vacuum heating (Brunel 1987) is the process. The vacuum heating mechanism vanishes when the plasma scale length surpasses the electromagnetic field skin depth. The $\boldsymbol{J} \times \boldsymbol{B}$ (Wilks *et al.* 1992) electron acceleration mechanism dominates with longer underdense pulse propagation. Self-focusing (Max, Arons & Langdon 1974) and other factors, including channel formation (Najmudin *et al.* 2003) which affects the energy coupling to electrons, modifies the laser pulse propagation in longer scale lengths. Recent simulations with $a_0 \gg 1$ and $n_e \gg n_c$ showed that ultraintense ($>10^{23}$ W cm^{-2}) laser–solid interactions generate a new electron acceleration mechanism called the zero-vector-potential (ZVP) absorption mechanism, which produces electrons with higher temperatures (Savin *et al.* 2019). The qualitative evidence of the ZVP mechanism can be seen graphically through high momentum spikes on the laser propagation axis. These spikes can verify that the high momentum of the electrons only occur for pulses where the vector potential passes through zero (Savin *et al.* 2017).

Such high laser irradiances of $I > 10^{23}$ W cm^{-2} generate extremely strong electromagnetic fields ($E_L \gtrsim 10^{15}$ V m^{-1}). These electromagnetic fields can accelerate electrons significantly, such that a large fraction of their energy is radiated as γ-rays, by nonlinear Compton scattering, within a single laser cycle, resulting in the radiation reaction (RR) force becoming vital in determining the electron trajectories (Dirac 1938). Thus, quantum aspects of the radiation emission are important (Kirk *et al.* 2009; Sokolov *et al.* 2010; Duclous, Kirk & Bell 2011) and electron–positron pairs can be generated by the emitted photons on interaction with the laser fields via multiphoton Breit–Wheeler pair production (Breit & Wheeler 1934; Bell & Kirk 2008; Fedotov *et al.* 2010). The plasma dynamics created by next generation 10 and 100 PW lasers will be dominated by these emission processes (Nerush *et al.* 2011; Sokolov, Naumova & Nees 2011; Ridgers *et al.* 2012). Quantum RR and multiphoton Breit–Wheeler pair production have a strong effect on particle acceleration in multipetawatt laser–solid interactions as shown in recent studies (Tamburini *et al.* 2010; Zhang, Ridgers & Thomas 2015). Current theoretical studies show that γ-ray and pair production can be done experimentally by using the flying mirror technique, which increases the laser pulse power up to the level where the laser electric field reaches the Schwinger limit at which electron positron pairs are produced (Bulanov *et al.* 2011).

Another important process in the interaction of lasers having $a_0 \gg 1$ with plasmas is relativistically induced transparency (RIT). In the ultrarelativistic regime, the effective mass of electrons in the plasma with high energies is much greater than the their rest mass. Therefore, the plasma frequency is reduced by a factor of $1/\sqrt{\langle\gamma\rangle}$, where $\langle\gamma\rangle$ is the average Lorentz factor of the electrons and the electron number density n_e is reduced by $1/\langle\gamma\rangle$. Consequently, an opaque plasma can be expected to become transparent if the $\langle\gamma\rangle$ is sufficiently high. This RIT (Palaniyappan *et al.* 2012) optically switches the plasma from opaque to transparent and enables light propagation. Thus, when the plasma frequency drops lower than the laser frequency, the laser propagates far behind the target because the light is no longer reflected at the critical surface (Lefebvre & Bonnaud 1995). Reaching this state with currently developed lasers requires foils thinner than a micron. These extreme laser intensities ($>10^{21}$ W cm^{-2}) turn the initially defined plasma into relativistically defined plasma and increases the mass of the electrons by the Lorentz factor $\langle\gamma\rangle = \sqrt{(1 + a_0^2/2)}$; subsequently, the critical plasma density turns to relativistic critical density ($n_{rc} = \gamma n_c$) which is far greater than our initially defined plasma density.

https://doi.org/10.1017/S0022377821000982 Published online by Cambridge University Press

Critical plasma density n_c can be defined as

$$n_{rc} = \gamma n_c, \quad n_c = \frac{4\pi^2 m_e \epsilon_0 c^2}{e^2} \frac{1}{\lambda^2} \simeq \frac{1.11 \times 10^{21}}{\lambda^2_{\mu m}} \mathrm{cm}^{-3}, \tag{1.3a,b}$$

where e and m_e are the electrical charge and rest mass of the electron, ϵ_0 is the free space permittivity and c is the speed of light. The measure of transparency or opaqueness of the plasma can be given with the equation (Vshivkov *et al.* 1998)

$$\zeta = \frac{\omega_p^2 l}{2\omega_L c} = \frac{\lambda l}{4\pi\delta^2}, \tag{1.4}$$

where l is the plasma thickness, ω_p and ω_L are the plasma and laser frequency, respectively, and δ is the plasma skin depth ($\delta = c/\omega_p$). The plasma is transparent when the dimensionless parameter $\zeta \ll 1$, but when $\zeta \gg 1$, the plasma is opaque. When the laser intensities $a_0 \gg 1$, a foil with $\zeta \gg 1$ is transparent as long as $a_0 \gg \zeta$. Our initial case before the interaction, $a_0 \simeq 483$, $\zeta \simeq 112$, shows that our plasma is transparent for the relativistic case which can be expressed as $\omega_L \gg \omega_p^2 l/2a_0 c$.

However, if we enter the QED-plasma regime as the electromagnetic fields increase, RR becomes important, the electron motion is damped and thus $\langle\gamma\rangle$ is expected to be reduced. Furthermore, RR leads to absorption of the electromagnetic wave (Mourou *et al.* 2006; Bashinov & Kim 2013).

Such high intensity lasers can accelerate ions with light pressure, known as radiation pressure acceleration (RPA) (Esirkepov *et al.* 2004; Robinson *et al.* 2008; Sorbo *et al.* 2018). The related radiation pressure can go up to $2I/c$, where I is the laser intensity and c is the speed of light. In this mechanism, the charge separation field leads the transfer of the radiation momentum to the accelerated ions. The electrons are pushed forward into the target (via radiation pressure) which causes a charge separation behind and generates an electrostatic field which accelerates background ions. In our simulations, we find that the laser bores a hole in the plasma due to the ponderomotive force as the laser pushes away electrons from the underdense region. This helps to create a dense local build-up of the electrons just beyond the critical layer, referred to as a snowplough (Sahai *et al.* 2013) as seen in figure 1. The electron snowplough forms only when the transparency conditions are valid and its speed is less than the laser group velocity $v_g/c = \sqrt{1 - n_e/n_c\gamma}$. For short laser pulses, ions stay undisturbed and effectively stationary by the ponderomotive force. In long scale length plasmas, this leads to a new ion acceleration mechanism, called relativistically induced transparency acceleration (RITA) (Sahai *et al.* 2013; Powell *et al.* 2015). The RITA mechanism is different than previously described laser–plasma ion acceleration mechanisms in several aspects. The background ions are mainly stable over the RITA time scales, whereas the ion motion is critical in other schemes (Gibbon 2000; Silva *et al.* 2004). In this mechanism, femtosecond relativistic laser pulses accelerate protons to produce quasimonoenergetic clusters with peak energies.

Recent studies have shown that QED effects reduce the energy of laser pulses in relativistically underdense plasmas with short-scale preplasma (1 μm), which is in disagreement with previous studies (plasmas without QED effects) where the preplasma actually becomes more transparent with increasing laser intensity (Wang *et al.* 2017).

To the best of our knowledge, in previous studies with QED particle-in-cell (PIC) simulations investigating the laser–plasma interactions at the multipetawatt level, a significant preplasma (up to 7 μm) has not been included and laser absorption mechanisms for protons and electrons with and without QED effects have not been compared at

https://doi.org/10.1017/S0022377821000982 Published online by Cambridge University Press

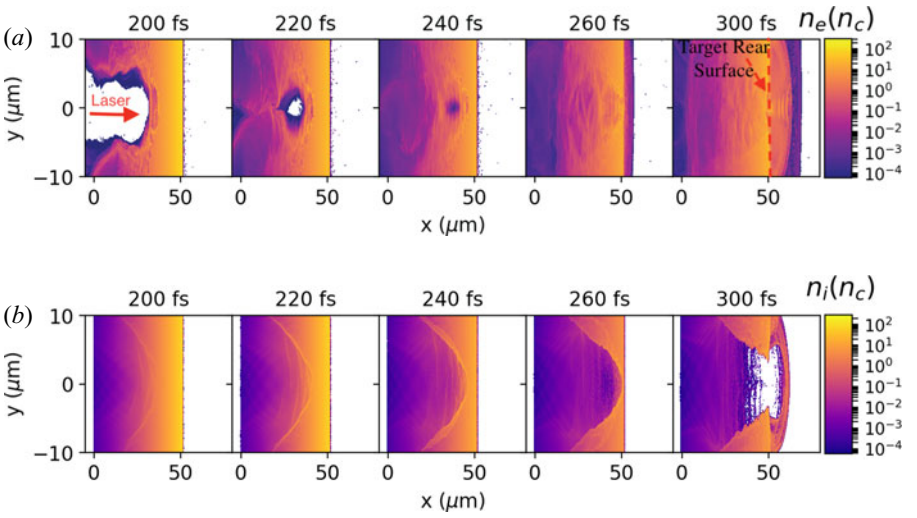

FIGURE 1. (*a*) Electron and (*b*) proton number densities for 5 μm scale length at several time steps, including QED effects.

different scale lengths (Brady, Ridgers & Arber 2012; Ridgers *et al.* 2012; Zhang *et al.* 2015; Kostyukov & Nerush 2016; Wang *et al.* 2017; Levy *et al.* 2019). We have employed the two-dimensional (2-D) EPOCH PIC code with the aforementioned QED effects (Ridgers *et al.* 2014; Arber *et al.* 2015). In reality, the laser prepulse will create a preplasma at the front surface of the target which dramatically increases electron acceleration efficiency (Culfa *et al.* 2014, 2016, 2017). Here, we investigate the effects of preformed plasma and nonlinear QED processes on particle acceleration in extreme laser plasma interactions ($I \sim 10^{23}$ W cm^{-2}).

2. EPOCH 2-D PIC code simulations

We used a 2-D EPOCH PIC code to simulate the laser–solid interactions with preformed plasma and QED effects on particle acceleration. The system size was 220 μm × 30 μm with a mesh resolution of 6875 × 1000 cells with each cell containing 100 electrons and 25 protons. The simulated laser irradiance was 5×10^{23} W cm^{-2} in a p-polarized beam with a 5 μm full width at half maximum (FWHM) focal spot and a laser incident angle of 0°. The laser wavelength and pulse duration were 0.8 μm and 30 fs, respectively. The solid hydrogen foil was chosen as a target and peak electron density was limited to $29n_c$ initially (Polz *et al.* 2019), where n_c is the critical density. In the case of preplasma, an exponential density profile was assumed with a maximum scale length of $L = 7$ μm and a cutoff to zero density at 0.001 n_c in front of a 1 μm foil. Plasma scale length L can be defined as $[-(\partial n_e/\partial x)/n_e]^{-1}$ where n_e is the electron number density.

We have performed simulations with QED, without QED and only with RR (where positron generation is artificially turned off) for several scale lengths ranging between 0 and 7 μm. Our simulations suggest particle acceleration mechanisms change when QED or RR is implemented. For irradiances greater than 10^{22} W cm^{-2}, we expect radiation pressure ion acceleration (RPA) (Esirkepov *et al.* 2004; Robinson *et al.* 2008; Tamburini *et al.* 2010) to be the dominating acceleration type mechanism of protons. However, in our simulations, we observed two different acceleration mechanisms – with and without QED – which impacted the plasma transparency.

https://doi.org/10.1017/S0022377821000982 Published online by Cambridge University Press

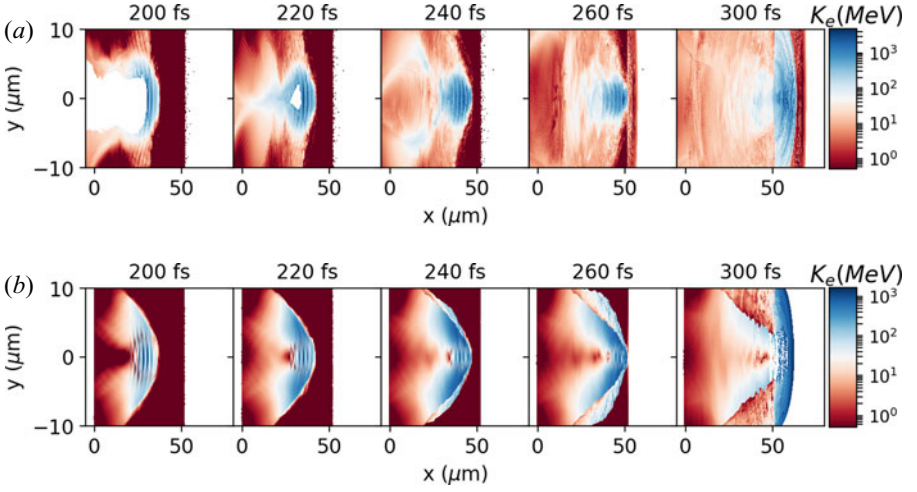

FIGURE 2. (*a*) Electron and (*b*) proton average kinetic energies for 5 μm scale length at several time steps, without QED effects.

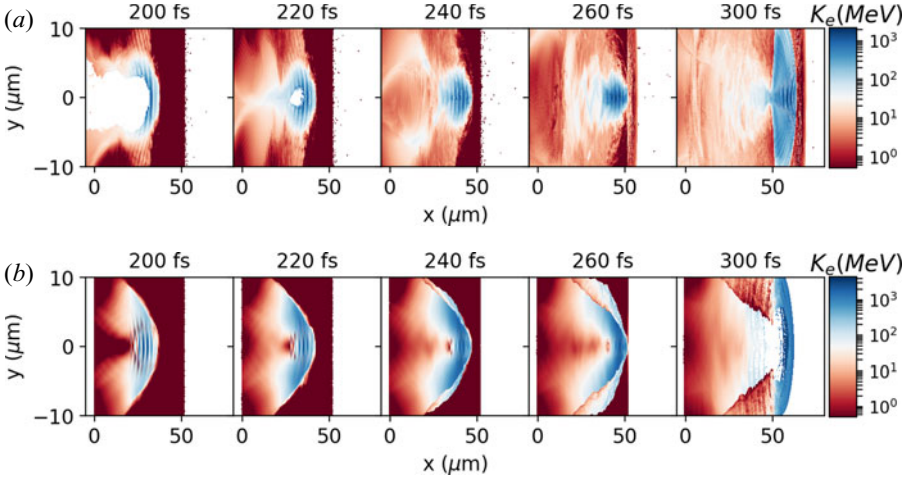

FIGURE 3. (*a*) Electron and (*b*) proton average kinetic energies for 5 μm scale length at several time steps, including QED effects.

Figure 2 shows the electron and ion average kinetic energy for $L = 5$ μm without QED effects. It can be seen that the ponderomotive force first pushes the electrons away and then the ions start gaining energy by light pressure (RPA mechanism). Figure 3 shows the electron, ion, photon and positron average kinetic energy for $L = 5$ μm with QED effects. It can be seen that, similar to figure 2, the initial acceleration mechanism and ion behaviour is similar to cases without QED effects. The accelerated electrons cause the acceleration of ions because of a moving electrostatic potential formed by an increase in the local electron density (RITA mechanism) at the later stage of the simulations. It can be seen that, especially for the RR case, there are monoenergetic ion beams produced for longer scale length cases ($L > 3$ μm). Figure 3 shows that initially ions and electrons accelerate and behave similarly to non-QED cases; however, with increasing time, their behaviours are changing due to the RITA mechanism, and monoenergetic ions are created. In the

https://doi.org/10.1017/S0022377821000982 Published online by Cambridge University Press

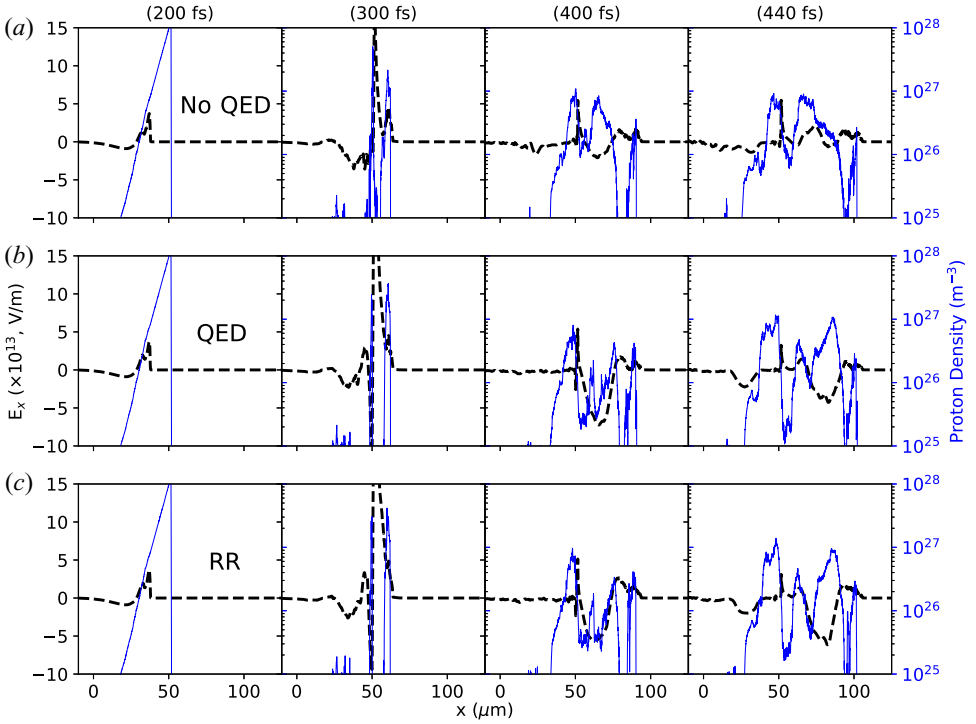

FIGURE 4. Longitudinal laser electric field (E_x) and proton number density for no QED, QED and only RR cases at different simulation time steps for $L = 5$ μm scale length.

electron-depleted region before the snowplough, a propagating electrostatic potential Φ_{sp} that follows the snowplough is set up due to the spatial charge separation between protons and electrons. If the potential difference is large enough, then protons can be picked up and accelerated to speeds twice that of the snowplough. Figure 4 shows the E_x longitudinal electric field due to charge separation which results in RITA acceleration when QED and RR is the process and the ions are moving with the longitudinal electric field. Figure 5 shows the proton longitudinal phase space on the x-axis for all three cases and all scale lengths at 400 fs time, where reflected RITA accelerated protons can be seen for the QED and RR-only cases. Similar to ions, we observed that electron acceleration mechanisms also have dependence on QED (or RR) effects. Figure 6 shows the longitudinal electron momentum on the x-axis ($P_x - x$) for all three cases and all plasma scale lengths at 400 fs time. One of the well known and proposed acceleration mechanisms when QED is implemented is $\boldsymbol{J} \times \boldsymbol{B}$ where electron oscillation frequency by the ponderomotive force is $2\omega_L$, where ω_L is the laser frequency (Wilks *et al.* 1992; Jiao *et al.* 2017). It is seen in figure 6 that the electron oscillation frequency is $2\omega_L$ ($d = \lambda/2$) which suggests that $\boldsymbol{J} \times \boldsymbol{B}$ is the main mechanism accelerating the electrons (see figure 6). However, we also noticed that without QED, there is another electron acceleration method involved in addition to the $\boldsymbol{J} \times \boldsymbol{B}$ electron acceleration mechanism. The observed momentum spikes of the electrons on the x-axis suggest that the ZVP acceleration mechanism is involved (see figure 6) (Savin *et al.* 2017). In the ZVP mechanism case, electrons are not directly accelerated by the $\boldsymbol{J} \times \boldsymbol{B}$ force, instead they are confined in a 'plasma capacitor' and perform finite oscillations which are much higher than the frequency of the relativistic electron oscillations caused by the ponderomotive force. The spatial duration of the

https://doi.org/10.1017/S0022377821000982 Published online by Cambridge University Press

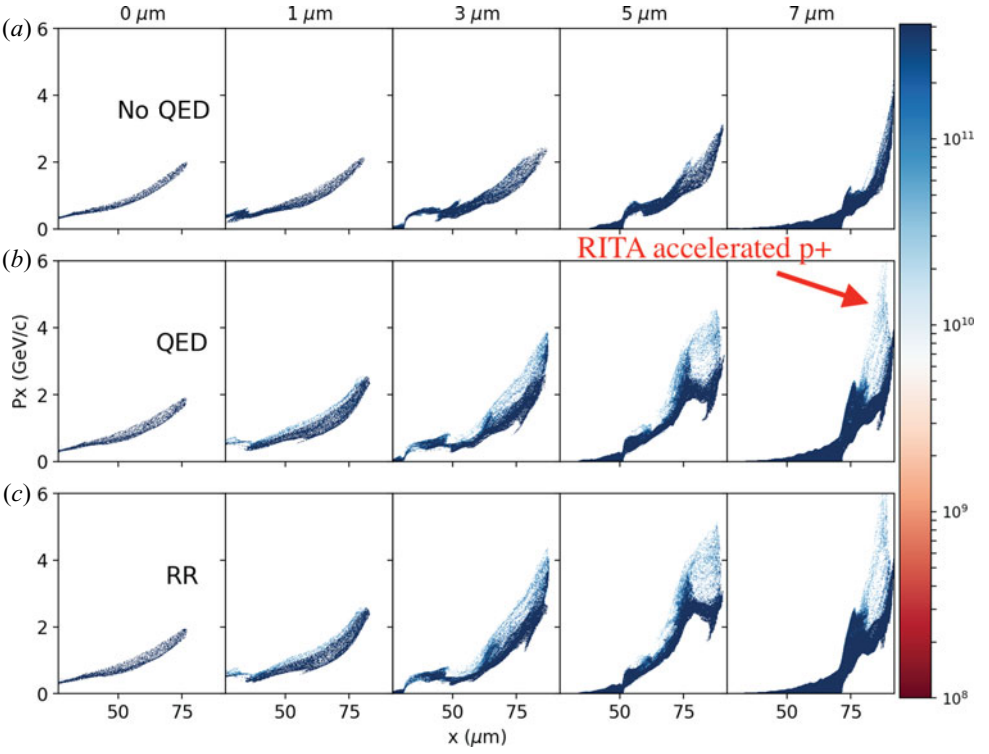

FIGURE 5. Proton phase space ($P_x - x$) distributions at different scale lengths for the cases of without (a) and with (b) the effects of QED and RR-only (c). Colourbar shows the weight of protons in arbitrary units.

electron cluster is given as $\Delta_{eb} \propto \lambda S/a_0^2$, where $S = n_e/n_c a_0$ which indicates that the fast electron clusters' spatial duration is much shorter than the period of the laser pulse (Baeva *et al.* 2011).

3. Energy spectra of accelerated particles

Electron, proton, γ-ray and positron energy spectra were examined in order to study the effects of both QED and plasma density scale length on particle acceleration. The energy spectra of electrons and protons at different time steps with a preformed plasma scale length L of 5 μm at the front surface are shown in figure 7 when QED effects are artificially switched off, switched on and when only RR effects are included (the laser is focused on $29n_c$ plasma slab at $t = 240$ fs for $L = 5$ μm case). It is seen that the accelerated particles' energy increased with time. Proton energy spectra shows that protons have a monoenergetic beam with increasing time and indicates that, the laser absorption mechanism changed during the simulation for the QED and RR cases. Figure 8 shows the energy spectra of electrons and protons with varied preformed plasma – extracted at the end of the simulation time ($t = 500$ fs) – for when QED effects are artificially switched off, switched on and when only the RR effect is included. When there is no preplasma ($L = 0$ μm), electron and ion energies reach a similar maximum energy for all cases. While electrons have continuous energy spectra in the cases of QED and RR-only, a peak is observed in the electron energy spectrum at around 2 GeV when QED is not included. However, increasing scale length ($L > 0$ μm) accelerates more energetic electrons for the

https://doi.org/10.1017/S0022377821000982 Published online by Cambridge University Press

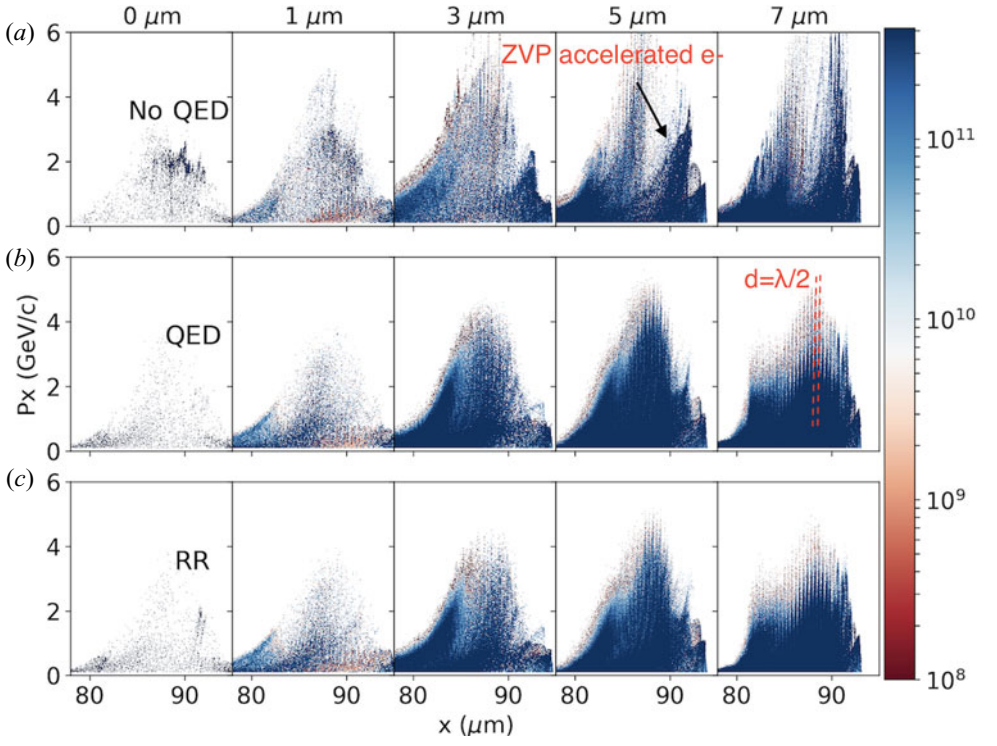

FIGURE 6. Electron phase space ($P_x - x$) distributions at different scale lengths for the cases of without (*a*) and with (*b*) the effects of QED and RR-only (*c*). Colourbar shows the weight of electrons in arbitrary units.

non-QED case, and higher energetic electrons (>4 GeV) are cooled down when the QED effect is more dominant. For the ions, it is clear that the QED and RR have a positive effect on ion acceleration which might be because of the increase in absorbed laser energy by ions (increase ∼2 % when QED and RR is on) or the change in the dominant ion acceleration mechanism from RPA to RITA.

For cases without QED effects, the electron energies are higher, while ion energies are lower when compared with RR and QED effect cases. However, QED effects cause significant cooling of very hot electrons while accelerating protons, as seen in figure 8. Results without QED effects show that increasing preplasma scale lengths ($L > 0$ μm) leads to more efficient laser absorption and, therefore, generates more energetic electrons and ions, as expected (Santala *et al.* 2000; Peebles *et al.* 2017). In the QED case, we see even stronger laser absorption as the preplasma scale length increases when compared with cases without QED effects, due to pair productions.

We have also performed simulations excluding pair production to determine whether RR or pair production has the stronger effect on particle acceleration. As shown in figure 8, QED and RR have a negligible effect on particle acceleration without preplasma, while RR is the key effect with preplasma. Pair production reduces the energy of accelerated ions as scale length increases. In the QED and RR cases, the energy of the accelerated electrons is reduced, while ions are accelerated to higher energies due to different dominant acceleration mechanisms caused by increased plasma opaqueness.

Comparing figures 8(*b*) and 8(*c*), one can see that hot electrons are cooled down by RR, which leads to significant absorption of the laser pulse and, therefore, a drop in

https://doi.org/10.1017/S0022377821000982 Published online by Cambridge University Press

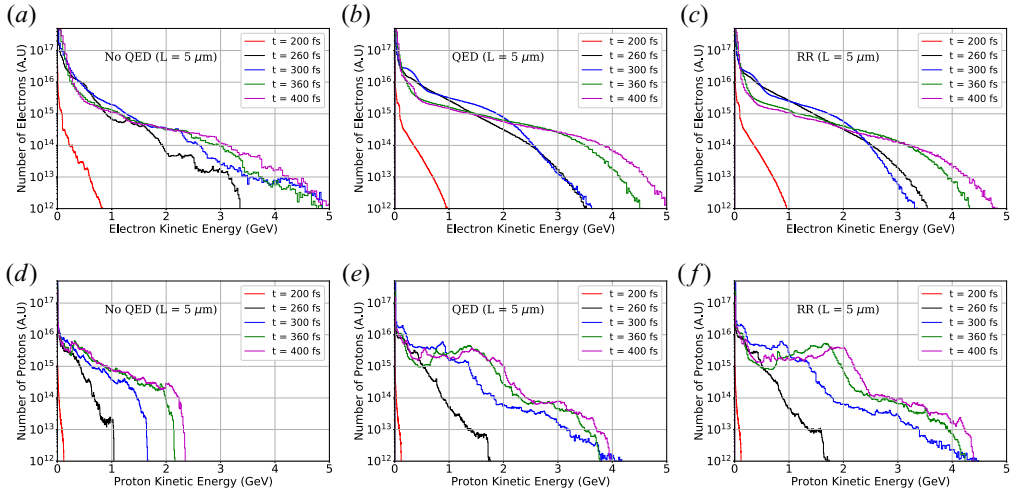

FIGURE 7. Electron (*a–c*) and proton (*d–f*) energy spectra for the cases of without (*a*,*d*) and with (*b*,*e*) the effects of QED and RR-only (*c*,*f*) for the $L = 5$ μm scale length case at different time steps.

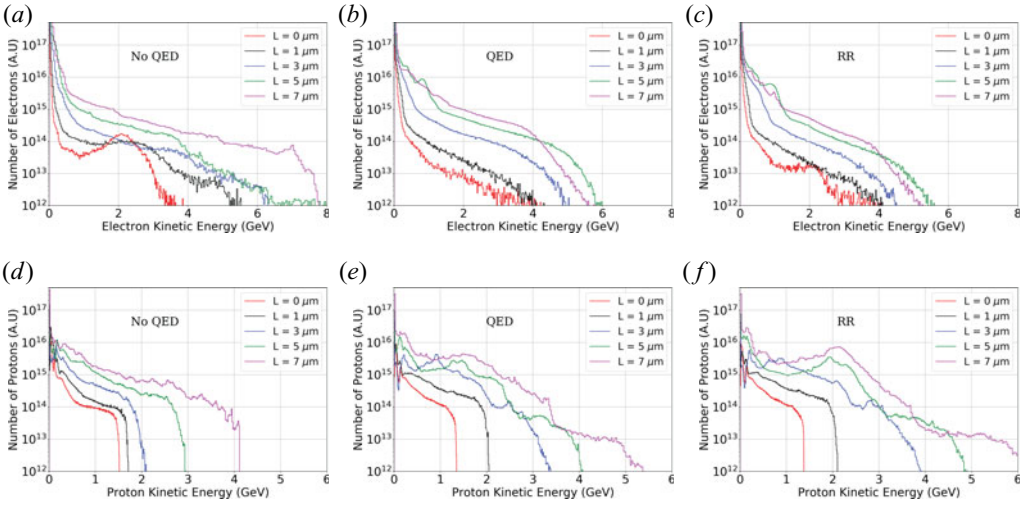

FIGURE 8. Electron (*a–c*) and proton (*d–f*) energy spectra for the cases of without (*a*,*d*) and with (*b*,*e*) the effects of QED and RR-only (*c*,*f*) for different scale lengths varying from 0 to 7 μm at the end of the simulation time.

the radiation pressure available to accelerate the protons by RPA (Sorbo *et al.* 2018) (see figures 8*d–f* and 9). This is due to extremely dense ($\approx 10^{23}$ cm^{-3}) pair-plasma when pair production is present.

In the QED-plasma regime, since the electromagnetic fields increase and RR becomes important, $\langle\gamma\rangle$ is expected to be reduced and RR helps to absorb more of the electromagnetic waves. Calculations for classical, semiclassical and QED plasmas show that γ is reduced when QED effects are included (Zhang *et al.* 2015). For the classical plasma (QED-off), $\gamma = \sqrt{1 + a_0^2}$. For the classical RR, dimensionless laser amplitude is

https://doi.org/10.1017/S0022377821000982 Published online by Cambridge University Press

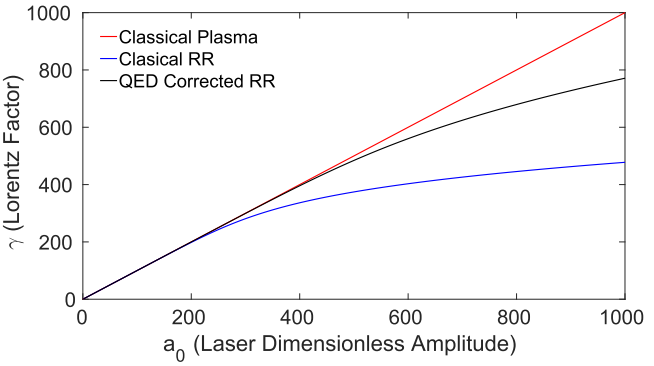

FIGURE 9. Radiation reaction effects on single electron dynamics are shown for classical plasma without RR effect (red line), for classical RR (blue line) and QED and for quantum corrected RR effect (black line).

given as:

$$a_0^2 = \tau_R^2 \omega_L^2 \gamma^8 + \gamma^2, \tag{3.1}$$

where τ_R is a production rate per electron per laser period and defined as $\tau_R = 0.06(I_{24}\lambda_{\mu m}^2)^{1/2}\eta^{1/4}\exp(-8/\sqrt{3\eta})$ and $\eta = \gamma E \sin\theta / E_s$ (Bell & Kirk 2008). For the relativistic plasma with QED effects, γ for the quantum corrected RR effects can be calculated from

$$\frac{\Gamma\gamma^2}{a_0^2} = \sqrt{1 - \frac{\gamma^2}{a_0^2}} \tag{3.2}$$

by using the definitions $\gamma = a_0 \sin\theta$ and $\Gamma \sin^2\theta - \cos\theta = 0$, where $\Gamma = \tau_R \omega_L a_0 \gamma^2$. By using (3.1) for classical RR, (3.2) for QED plasma and $\gamma = \sqrt{1 + a_0^2}$ for classical plasma, we can obtain the plot given in figure 9 and can show the reduction in γ values for QED plasmas which affects the plasma opaqueness.

Figure 10 shows the total laser energy (E_L) – propagated in the x direction – and plasma electron number density when QED is off, on and RR-only cases at different simulation times for $L = 5$ μm scale length. It is seen that without QED, the ponderomotive force pushes the particles away but the laser absorption is lower when compared with QED and RR cases due to RIT. In our simulations, the plasma becomes totally transparent and there is very little laser reflection ($n_{rc} = 5.86 \times 10^{23}$ cm^{-3}). Laser absorption is around 8 % without QED and 30 % with QED. In particular, for the cases without QED, at the maximum plasma scale length of $L = 7$ μm, the laser absorption is only ∼10 % and the rest of the laser passes through the target. When QED is turned on, laser absorption increases dramatically, mainly due to RR caused by γ-ray radiation (which is around 24 % conversion efficiency for the $L = 7$ μm case).

Figure 11 shows the laser E_y electric field before and after laser focusing for cases without and with QED effects. It is seen that the laser is self-focused in both cases due to long plasma scale lengths of up to a few μm FWHM, which increases the initially defined laser intensity up to ∼10^{24} W cm^{-2} for all cases. While laser self-focusing does have an effect on accelerating particles, because of its very similar character in all cases, we can neglect this effect in our comparisons.

Figure 12 shows the energy spectra of generated photons for different preformed plasma scale lengths with QED and RR. Preformed plasma increases the energy of generated photons. Previous studies showed that there is a threshold limit for the photon energy with

https://doi.org/10.1017/S0022377821000982 Published online by Cambridge University Press

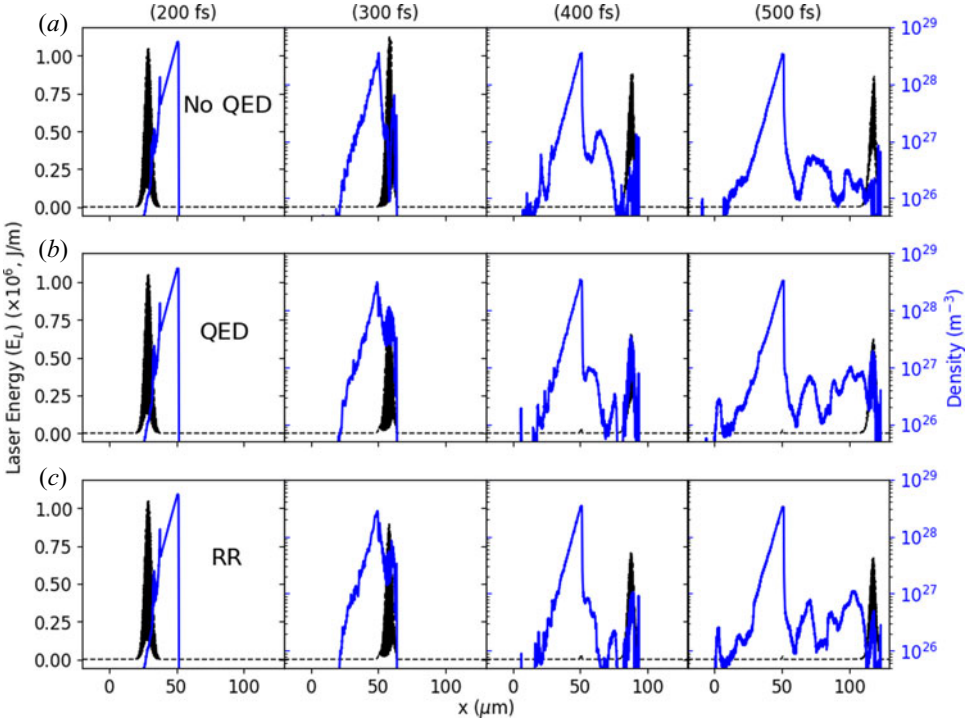

FIGURE 10. Laser energy E_L and plasma number density without QED, with QED and only RR cases at different simulation time steps for $L = 5$ μm scale length.

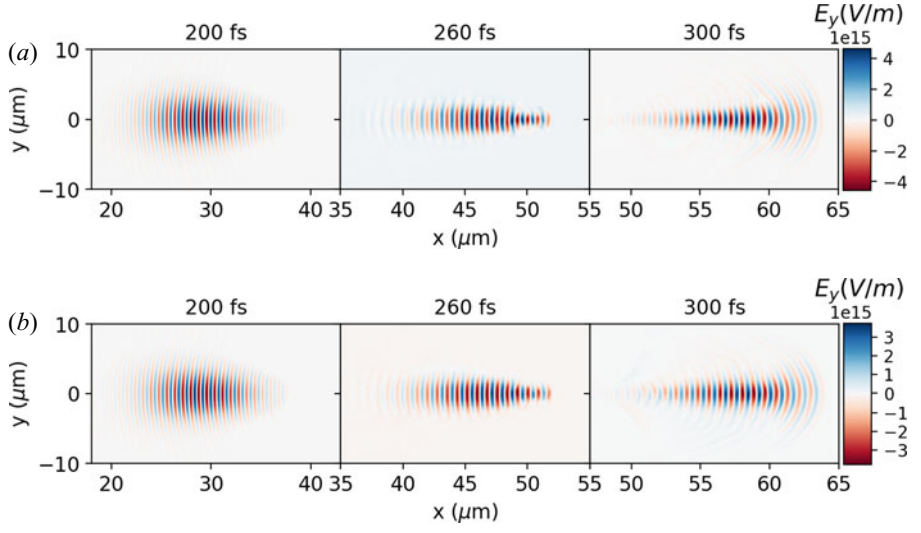

FIGURE 11. The E_y laser electric field for 5 μm scale length at several time steps (*a*) without QED and (*b*) with QED cases.

increasing scale length and that for 30 fs, ∼10 PW laser systems, the gamma conversion rate is at a maximum when the scale length is around $L \simeq 20$ μm but if the laser pulse duration is longer (150 fs), optimum plasma scale length is reduced to $L \simeq 10$ μm (Lezhnin *et al.* 2018). The generated photon energies are slightly higher in the QED cases

https://doi.org/10.1017/S0022377821000982 Published online by Cambridge University Press

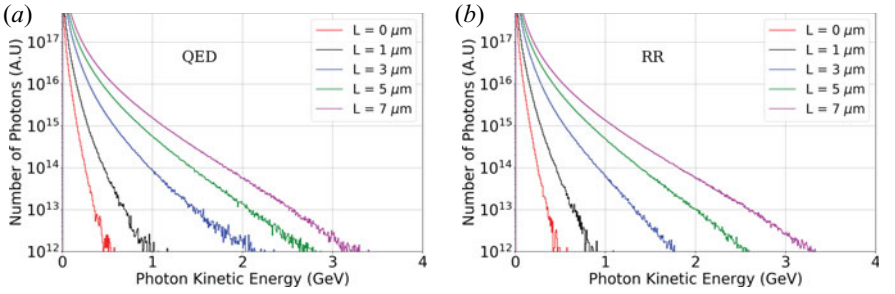

FIGURE 12. Photon energy spectra with QED (*a*) and RR (*b*) effects for several plasma scale lengths.

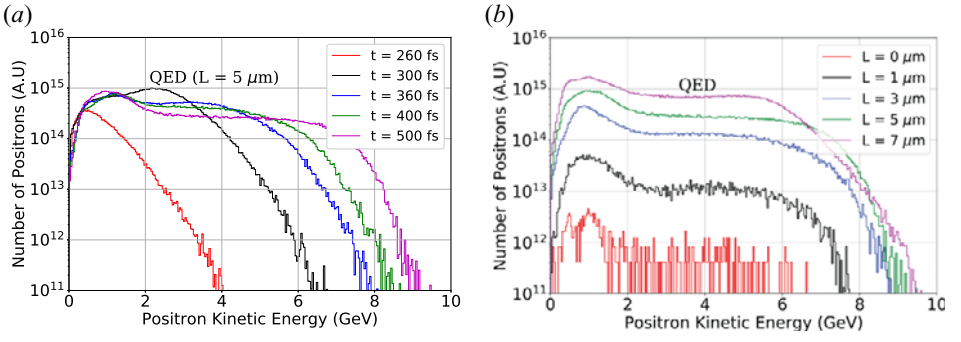

FIGURE 13. Positron energy spectra for (*a*) several different time steps when $L = 3$ μm and (*b*) for several plasma scale lengths at the end of the simulation ($t = 500$ fs).

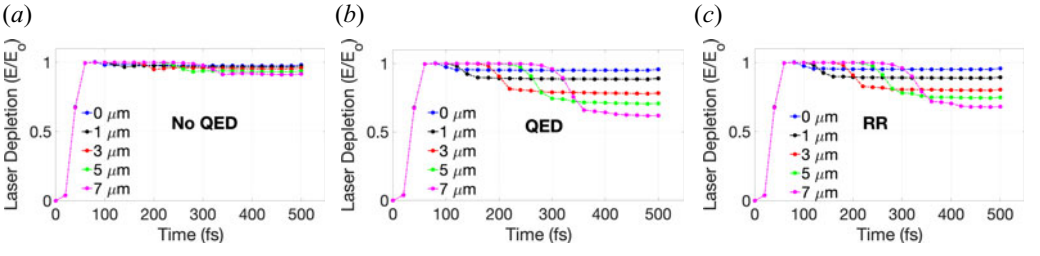

FIGURE 14. The conversion efficiency of intense laser pulse into energetic particles via absorption for no QED (*a*), QED (*b*) and RR (*c*) cases at different scale lengths.

due to the density of relativistic plasma and laser conversion efficiency, which is 24 % in the QED case (21 % for RR cases) when $L = 7$ μm.

The generated positron energy spectra for different plasma scale lengths are shown in figure 13. Adding a preformed plasma in next generation laser–solid interactions leads to the generation of higher energy photons and positrons (Nakamura *et al.* 2012). Initially, for all cases, the results are not surprising with preformed plasma, since the accelerated electrons are more energetic. In the QED cases the positrons can, just as the electrons, be accelerated in the preformed plasma to higher energies, as seen in figure 13. Laser–positron conversion efficiency increases with increasing plasma scale length up to ∼4 %.

Figure 14 shows the conversion efficiency of intense laser pulses into energetic particles – via absorption – for no QED, QED and RR cases at different scale lengths.

https://doi.org/10.1017/S0022377821000982 Published online by Cambridge University Press

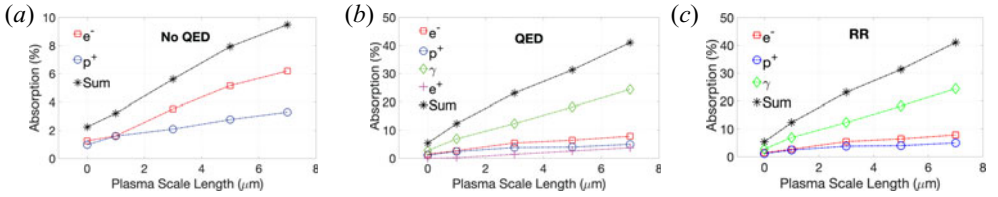

FIGURE 15. Total laser absorption by the plasma and by the particles inside the plasma as a function of plasma scale length for the cases with no QED (*a*), QED (*b*) and RR (*c*) at different scale lengths.

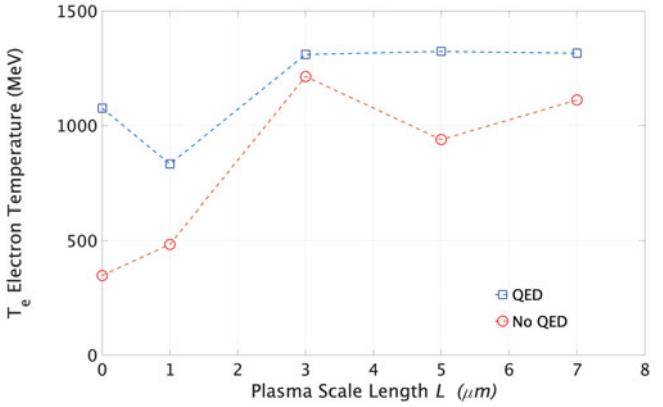

FIGURE 16. Calculated electron temperature T_e as a function of plasma scale length with (□, blue) and without (○, red) QED cases.

It is seen that QED and RR-only effects increase the plasma opacity and cause higher laser absorption (up to 40 % when $L = 7$ μm mainly by γ-rays). We also show the laser absorption by each particle species and the total conversion efficiency as a function of plasma scale length in figure 15.

Figure 15 shows the total laser absorption as a function of plasma scale length for the cases with QED, without QED and RR-only. The results in this work are consistent with those quoted in Levy *et al.* (2019), where total laser absorption efficiency is around 40 % with the laser intensities 10^{23} W cm^{-2}. Our studies show the importance of target design, i.e. adding preformed plasma to increase the efficiency of γ-ray generation for the future laser plasma experiments.

Figure 16 shows the extracted electron temperature with and without QED effects as a function of plasma scale length. We determined the electron temperature (kT_e) by fitting the hot tail of electron spectra with an exponential function of the form $\exp(-E/kT_e)$. For such intensities, if the QED effect is not taken into account, the calculated temperature has a similar trend in terms of having an optimum temperature, which is at $L = 3$ μm in this study, whereas it was measured $L \simeq 8$ μm experimentally with lower laser irradiances ($\sim 10^{20}$ W cm^{-2}) due to laser filamentation and absorption in longer preformed plasmas (Culfa *et al.* 2014, 2016). However, the hot electron temperature T_e follows a different trend when QED effects are present. Our results show that if there is no scale length, the number of generated hot electrons is lower when compared with $L > 0$ μm scale length cases. When there is a preformed plasma with a scale length of $L = 1$ μm, more electrons are generated but their temperatures are decreased. However, increasing scale length helps generate more electrons with higher temperatures due to increased plasma opacity (caused

https://doi.org/10.1017/S0022377821000982 Published online by Cambridge University Press

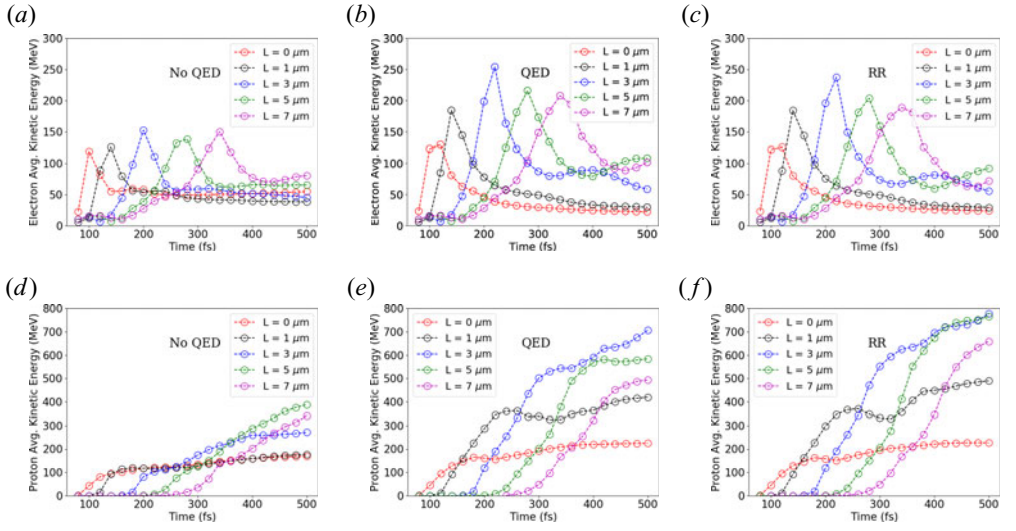

FIGURE 17. Electron (*a–c*) and proton (*d–f*) average energy for the cases without (*a–d*) and with (*b–e*) the effects of QED and RR-only (*c–f*) as a function of time for several scale lengths.

by QED effects). Recent studies show that if the QED effect is in the process, electron temperature (T_e) is proportional to normalized laser amplitude (a_o). Savin *et al.* (2019) claims that $T_e \propto a_o^2$ without QED and $T_e \propto a_o^5$ with QED effects. Since a small fixed amount of scale length ($L = 0.2$ μm) was used in their simulations, Savin *et al.* did not take into account the effect of varied preformed plasma scale length, which has a high impact on electron acceleration calculations. Our studies are in agreement with the Savin *et al.* (2019) calculated results for corresponding $a_o \sim 483$ and L scale length between 0 and 1 μm with and without QED cases.

Figure 17 shows average electron and proton energies as a function of time for non-QED, QED and RR-only cases. Optimum scale length is found to be around 3 μm for electron and proton acceleration. Since the average photon energy is nearly the same for QED and RR cases, as seen in figure 18, it is understood that RR is the effect which accelerates charged particles to higher energies for extreme laser intensities. When there is an absence of preplasma ($L = 0$ μm), no QED, QED and RR have similar trends for ion acceleration due to the lack of photon and positron generation. Accelerated protons reach their maximum average energy at ∼150 fs and remain almost constant until the end of the simulation, indicating that QED and RR effects are very small.

With increasing scale length, QED and RR effects help to accelerate more electrons with moderate energies (1–4 GeV), while in No-QED cases only a small fraction of electrons are accelerated to very high energies (>4 GeV). Although very hot electrons are cooled down with QED effects, the average energy increases due to a larger fraction of electrons being at moderate energies.

When preplasma is present, QED and RR cases show that ions are accelerated dramatically up to some point (depending on scale length) then continue to accelerate with a smaller growth until the end of the simulation due to effects of plasma opacity. Figure 18 shows that photons gain energy, then start losing their energy before a point at which the ions have a second acceleration increase which emphasizes that RR has an effect on ion heating by increasing plasma opacity. The drop in the average energy of photons indicates that the number of generated γ-rays are increasing with energies below 1 GeV.

https://doi.org/10.1017/S0022377821000982 Published online by Cambridge University Press

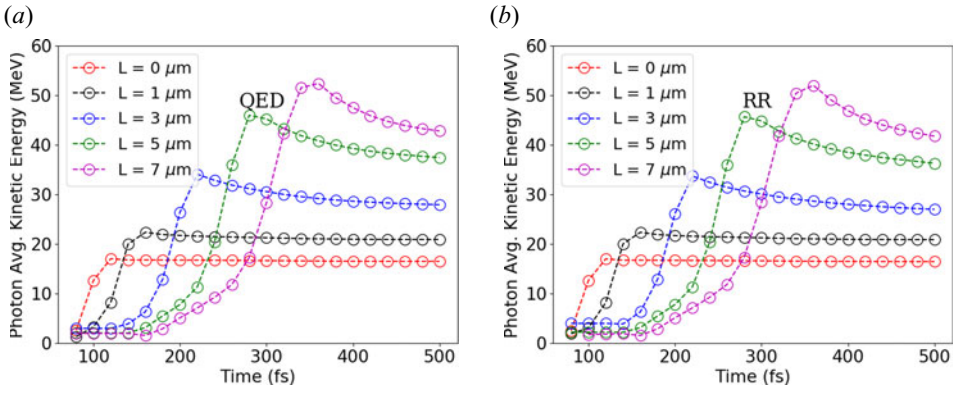

FIGURE 18. Average photon energy as a function of time with QED (*a*) and RR-only (*b*) effects for several plasma scale lengths.

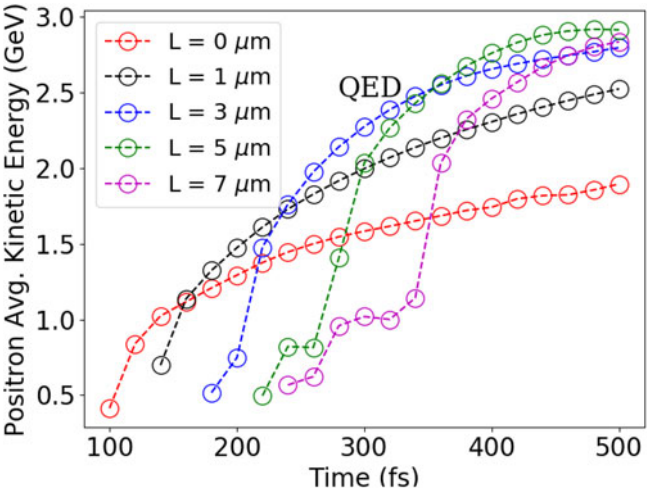

FIGURE 19. Average positron energy as a function of time for several scale lengths.

Figure 19 shows the average positron energy generated through nonlinear QED effects during the laser plasma interactions with different preformed plasma scale lengths. When the number of positrons is increased with increasing scale length, QED effects become important and the amount of laser absorption inside the plasma starts increasing, while the energy of accelerated protons decreases (when compared with the RR-only case), as shown in figures 8, 13 and 19.

4. Angular distribution of ions

The angular distribution of charged particles has significant importance for future applications. Figure 20 shows the angular distribution of the accelerated ions behind the target with kinetic energies greater than 0.5 MeV for different plasma scale lengths with and without QED and RR effects. We see that increasing plasma scale length helps to accelerate more collimated ion beams with higher energies when there is no QED effect. It shows that RPA is in the process and accelerates more focused, higher energy ions without QED effects. However, once the QED (or RR) is introduced to our simulations,

https://doi.org/10.1017/S0022377821000982 Published online by Cambridge University Press

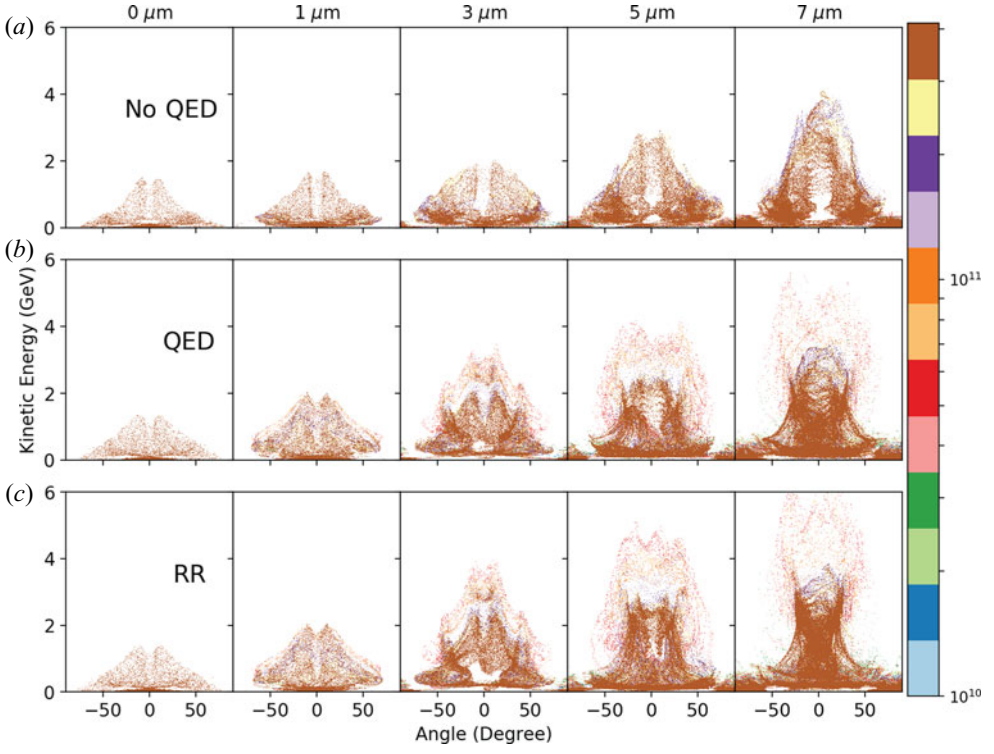

FIGURE 20. Proton angular distributions at different scale lengths for the cases of without (*a*) and with (*b*) the effects of QED and RR-only (*c*). Colourbar shows the weight of protons in arbitrary units.

RPA is changing to RITA acceleration which spreads out the collimated ion beam (proton reflection). Increasing plasma scale length still helps generate more energetic ions with QED and RR cases. However, for scale lengths greater than 3 μm, higher laser absorption is observed due to high photon and positron generation. Ions are heated by the RITA acceleration mechanism and, therefore, accelerated ions scatter around so their angular distribution is increased and they are no longer collimated. It is clear that QED or RR-only will be the more effective case for future laser–plasma experiments with higher laser intensities in next generation laser facilities. Generating a high energy focused proton beam is essential for accelerated ion applications. Our study shows that if QED or RR is in the process for future experimental studies, the optimum plasma scale length L should be around 3 μm in order to be used in different applications.

5. Conclusion

In conclusion, we investigated the effect of plasma scale length and QED processes on particle acceleration and the angular distribution of protons in laser–matter interactions for laser intensities of 5×10^{23} W cm^{-2}. On simulating the case with varied preformed plasma scale length, we have found that in the case without QED, more efficient laser absorption occurs due to the preformed plasma and generated electrons and ions having more energy compared with cases without preplasma. However, in the case where QED is included, physical mechanisms change and strong laser absorption in the preplasma reverses this trend. That is, the hot electrons are cooled down due to QED effects, whereas

https://doi.org/10.1017/S0022377821000982 Published online by Cambridge University Press

ions have more energy due to the new dominant laser absorption mechanism (RITA) and the increase in laser energy conversion efficiency.

We have also found that the electron energy is reduced due to RR, but in the case of no scale length, QED processes (RR and pair production from the emitted photons) have no effect since the generated number of photons and positrons is minimal. For QED processes with scale lengths, pair production significantly affected the particles' energy; the increase in the particles' energy is mainly because of RR effects which increase plasma opacity. We have shown that more energetic γ-rays and positrons are created with increasing scale length due to high laser conversion efficiency (24 % for photons and 4 % for positrons for $L = 7\ \mu$m) which affected our ion and electron acceleration mechanisms. The QED effect also has an important impact on ion angular distribution. We showed that if there is no QED effect, ions are collimated more, but the QED effect scatters ions due to the different laser absorption mechanism (RITA) and less collimated angular distribution is obtained. For the best collimated ion beam, $L \leqslant 3\mu$ m scale length should be achieved.

Acknowledgements

We would like to thank Dr C. Ridgers for his useful comments and feedback. We also would like to thank S. North for proofreading.

Editor Victor Malka thanks the referees for their advice in evaluating this article.

Funding

The research was supported by TUBITAK (grant number 118F077). This work was in part funded by the UK EPSRC (grant numbers EP/G054950/1, EP/G056803/1, EP/G055165/1, EP/M018156/1, EP/ M022463/1).

Declaration of interests

The authors report no conflict of interest.

REFERENCES

Albright, B., Yin, L., Bowers, K.J., Hegelich B.M., Flippo K.A., Kwan T.J.T. & Fernández J.C. 2007 Relativistic buneman instability in the laser breakout afterburner. *Phys. Plasmas* **14**, 094502.

Arber, T., Bennett, K., Brady, C., Lawrence-Douglas A., Ramsay M.G., Sircombe N.J., Gillies P., Evans R.G., Schmitz H., Bell A.R. & Ridgers C.P. 2015 Contemporary particle-in-cell approach to laser-plasma modelling. *Plasma Phys. Control. Fusion* **57**, 113001.

Baeva, T., Gordienko, S., Robinson, A. & Norreys, P. 2011 Efficient laser-driven proton acceleration from a cryogenic solid hydrogen target. *Phys. Plasmas* **18**, 056702.

Bashinov, A. & Kim, A. 2013 On the electrodynamic model of ultra-relativistic laser-plasma interactions caused by radiation reaction effects. *Phys. Plasmas* **20**, 113111.

Bell, A. & Kirk, J. 2008 Possibility of prolific pair production with high-power lasers. *Phys. Rev. Lett*. **101**, 200403.

Blaga, C., Xu, J., DiChiara, A., Sistrunk E., Zhang K., Agostini P., Miller T.A., DiMauro L.F. & Lin C.D. 2011 Imaging ultrafast molecular dynamics with laser-induced electron diffraction. *Nature* **483**, 194–197.

Brady, C., Ridgers, C., Arber, T., Bell A.R. & Kirk J.G. 2012 Laser absorption in relativistically underdense plasmas by synchrotron radiation. *Phys. Rev. Lett*. **109**, 245006.

Breit, G. & Wheeler, J.A. 1934 Collision of two light quanta. *Phys. Rev*. **46**, 1087.

Brunel, F. 1987 Not-so-resonant, resonant absorption. *Phys. Rev. Lett*. **59**, 52–55.

Bulanov, S., Esirkepov, T., Hayashi, Y., Kando M., Kiriyama H., Koga J.K., Kondo K., Kotaki H., Pirozhkov A.S., Bulanov S.S., *et al.* 2011 On the design of experiments for the

https://doi.org/10.1017/S0022377821000982 Published online by Cambridge University Press

study of extreme field limits in the interaction of laser with ultrarelativistic electron beam. *Nucl. Instrum. Meth. Phys. Res*. **660**, 31–42.

BULANOV, S.V., WILKENS, J.J., ESIRKEPOV, T., KORN G., KRAFT G., KRAFT S.D., MOLLS M. & KHOROSHKOV V.S. 2014 Laser ion acceleration for hadron therapy. *Phys. Uspekhi* **57**, 1149–1179.

CULFA, O., TALLENTS, G.J., KORKMAZ, M., ROSSALL A.K., WAGENAARS E., RIDGERS C.P., MURPHY C.D., BOOTH N., CARROLL D.C., WILSON L.A., *et al.* 2017 Plasma scale length effects on protons generated in ultra intense laser plasmas. *Laser Particle Beams* **35**, 58–63.

CULFA, O., TALLENTS, G.J., ROSSALL, A.K., WAGENAARS E., RIDGERS C.P., MURPHY C.D., DANCE R.J., GRAY R.J., MCKENNA P., BROWN C.D.R., *et al.* 2016 Plasma scale-length effects on electron energy spectra in high-irradiance laser plasmas. *Phys. Rev. E* **93**, 043201.

CULFA, O., TALLENTS, G.J., WAGENAARS, E., RIDGERS C.P., DANCE R.J., ROSSALL A.K., GRAY R.J., MCKENNA P., BROWN C.D.R., JAMES S.F., *et al.* 2014 Hot electron production in laser solid interactions with a controlled pre-pulse. *Phys. Plasmas* **21**, 043106.

DAIDO, H., NISHIUCHI, M. & PIROZHKOV, A. 2012 Review of laser-driven ion sources and their applications. *Rep. Prog. Phys*. **75**, 056401.

DANSON, C.N., HAEFNER, C., BROMAGE, J., BUTCHER T., CHANTELOUP J-C. F., CHOWDHURY E.A., GALVANAUSKAS A., GIZZI L.A., HEIN J., HILLIER D.I., *et al.* 2019 Petawatt and exawatt class lasers worldwide. *High Power Laser Sci. Engng* **7**, e54.

DIRAC, P. 1938 Classical theory of radiating electrons. *Proc. R. Soc. Lond.* A **167**, 148.

DUCLOUS, R., KIRK, J. & BELL, A. 2011 Monte Carlo calculations of pair production in high-intensity laser–plasma interactions. *Plasma. Phys. Control. Fusion* **53**, 015009.

ESAREY, E., SCHROEDER, C. & LEEMANS, W. 2009 Physics of laser-driven plasma-based electron accelerators. *Rev. Mod. Phys*. **81**, 1229–1285.

ESIRKEPOV, T., BORGHESI, M., BULANOV, S., MOUROU G. & TAJIMA T. 2004 Highly efficient relativistic-ion generation in the laser-piston regime. *Phys. Rev. Lett*. **92**, 175003.

ESIRKEPOV, T., KOGA, J., SUNAHARA, A., MORITA, T., NISHIKINO, M., KAGEYAMA, K., NAGATOMO, H., NISHIHARA, K., SAGISAKA, A., KOTAKI, H., *et al.* 2014 Prepulse and amplified spontaneous emission effects on theinteraction of a petawatt class laser with thin solid targets. *Nucl. Instrum. Meth. Phys. Res*. **745**, 150–163.

FEDOTOV, A., NAROZHNY, N.B., MOUROU, G. & KORN G. 2010 Limitations on the attainable intensity of high power lasers. *Phys. Rev. Lett*. **105**, 080402.

GIBBON, P. 2000 *Short Pulse Laser Interactions with Matter*. Imperial College Press.

HADJISOLOMOU, P., TSYGVINTSEV, I., SASOROV, P., GASILOV, V., KORN, G. & BULANOV, S. 2020 Preplasma effects on laser ion generation from thin foil targets. *Phys. Plasmas* **27**, 013107.

JIAO, J., ZHANG, B., YU, J. , ZHANG Z., YAN Y., HE S., DENG Z., TENG J., HONG W. & GU Y. 2017 Generating high-yield positrons and relativistic collisionless shocks by 10 PW laser. *Laser Particle Beams* **35**, 234–240.

JUNG, D., YIN, L., GAUTIER, D., WU H.-C., LETZRING S., DROMEY B., SHAH R., PALANIYAPPAN S., SHIMADA T., JOHNSON R.P., *et al.* 2013 Laser-driven 1 GeV carbon ions from preheated diamond targets in the break-out afterburner regime. *Phys. Plasmas* **20**, 083103.

KIRK, J., BELL, A. & ARKA, I. 2009 Pair production in counter-propagating laser beams. *Plasma Phys. Control. Fusion* **51**, 085008.

KNEIP, S., NAGEL, S., MARTINS, S., MANGLES S.P.D., BELLEI C., CHEKHLOV O., CLARKE R.J., DELERUE N., DIVALL E.J., DOUCAS G., *et al.* 2009 Near-GeV acceleration of electrons by a nonlinear plasma wave driven by a self-guided laser pulse. *Phys. Rev. Lett*. **103** (3), 035002.

KOSTYUKOV, I. & NERUSH, E. 2016 Production and dynamics of positrons in ultrahigh intensity laser-foil interactions. *Phys. Plasmas* **23**, 093119.

KRUER, W. 1988 *The Physics of Laser Plasma Interactions*. Addison-Wesley.

LEEMANS, W., NAGLER, B., GONSALVES, A., TÓTH CS., NAKAMURA K., GEDDES C.G.R., ESAREY E., SCHROEDER C.B. & HOOKER S.M. 2006 GeV electron beams from a centimetre-scale accelerator. *Nat. Phys*. **2**, 696–699.

LEFEBVRE, E. & BONNAUD, G. 1995 Transparency/opacity of a solid target illuminated by an ultrahigh-intensity laser pulse. *Phys. Rev. Lett*. **74**, 2002.

Levy, M., Blackburn, T., Ratan, N., Sadler J., Ridgers C.P., Kasim M., Ceurvorst L., Holloway J., Baring M.G., Bell A.R., *et al.* 2019 QED-driven laser absorption. arXiv:1609.00389v2 [physics.plasm-ph].

Lezhnin, K., Sasorov, P., Korn, G. & Bulanov, S. 2018 High power gamma flare generation in multi-petawatt laser interaction with tailored targets. *Phys. Plasmas* **25**, 123105.

Macchi, A., Borghesi, M. & Passoni, M. 2013 Ion acceleration by superintense laser-plasma interaction. *Rev. Mod. Phys*. **85**, 751–793.

Max, C., Arons, J. & Langdon, A. 1974 Self-modulation and self-focusing of electromagnetic waves in plasmas. *Phys. Rev. Lett*. **33**, 209–212.

McKenna, P., Carroll, D., Lundh, O., Nürnberg F., Markey K., Bandyopadhyay S., Batani D., Evans R.G., Jafer R., Kar S., *et al.* 2008 Effects of front surface plasma expansion on proton acceleration in ultraintense laser irradiation of foil targets. *Laser Particle Beams* **26** (4), 591–596.

Mourou, G., Tajima, T. & Bulanov, S. 2006 Optics in the relativistic regime. *Rev. Mod. Phys*. **78**, 309.

Najmudin, Z., Krushelnick, K., Tatarakis, M., Clark E.L., Danson C.N., Malka V., Neely D., Santala M.I.K. & Dangor A.E. 2003 The effect of high intensity laser propagation instabilities on channel formation in underdense plasmas. *Phys. Plasmas* **10**, 438.

Nakamura, T., Koga, J., Esirkepov, T.Z. , Kando M., Korn G. & Bulanov S.V. 2012 High-power γ-ray flash generation in ultraintense laser-plasma interactions. *Phys. Rev. Lett*. **108**, 195001.

Nerush, E.N., Kostyukov, I.Y., Fedotov, A.M., Narozhny N.B., Elkina N.V. & Ruhl H. 2011 Laser field absorption in self-generated electron-positron pair plasma. *Phys. Rev. Lett*. **106**, 035001.

Palaniyappan, S., Hegelich, B.M., Wu, H., Jung, D., Gautier, D., Yin, L., Albright, B., Johnson, R., Shimada, T., Letzring, S., *et al.* 2012 Dynamics of relativistic transparency and optical shuttering in expanding overdense plasmas. *Nat. Phys*. **8**, 763–769.

Peebles, J., Wei, M., Arefiev, A., McGuffey C., Stephens R.B., Theobald W., Haberberger D., Jarrott L.C., Link A., Chen H., *et al.* 2017 Investigation of laser pulse length and pre-plasma scale length impact on hot electron generation on omega-ep. *New J. Phys*. **19**, 023008.

Piazza, A.D., Muller, C., Hatsagortsyan, K. & Keitel C.H. 2012 Extremely high-intensity laser interactions with fundamental quantum systems. *Rev. Mod. Phys*. **84**, 1177.

Polz, J., Robinson, A., Kalinin, A., Becker G.A., Costa Fraga R.A., Hellwing M., Hornung M., Keppler S., Kessler A., Klöpfel D., *et al.* 2019 Efficient laser-driven proton acceleration from a cryogenic solid hydrogen target. *Sci. Rep*. **9**, 16534.

Powell, H., King, M., Gray, R., MacLellan D.A., Gonzalez-Izquierdo B., Stockhausen L.C., Hicks G., Dover N.P., Rusby D.R., Carroll D.C., *et al.* 2015 Proton acceleration enhanced by a plasma jet in expanding foils undergoing relativistic transparency. *New J. Phys*. **17**, 103033.

Qiao, B., Kar, S., Geissler, M., Gibbon P., Zeph M. & Borghesi M. 2012 Dominance of radiation pressure in ion acceleration with linearly polarized pulses at intensities of 10^{21} W cm^{-2}. *Phys. Rev. Lett*. **108**, 115002.

Ridgers, C., Brady, C., Duclous, R., Kirk J.G., Bennett K., Arber T.D., Robinson A.P.L. & Bell A.R. 2012 Dense electron-positron plasmas and ultraintense γ rays from laser-irradiated solids. *Phys. Rev. Lett*. **108**, 165006.

Ridgers, C., Kirk, J., Duclous, R., Blackburn T.G., Brady C.S., Blackburn K., Arber T.D. & Bell A.R. 2014 Modelling gamma-ray photon emission and pair production in high-intensity laser–matter interactions. *J. Comput. Phys*. **260**, 273–285.

Robinson, A., Zepf, M., Kar, S., Evans R.G. & Bellei C. 2008 Radiation pressure acceleration of thin foils with circularly polarized laser pulses. *New J. Phys*. **10**, 01302.

Sadighi-Bonabi, R., Yazdani, E., Cang, Y. & Hora H. 2010 Dielectric magnifying of plasma blocks by nonlinear force acceleration with delayed electron heating. *Phys. Plasmas* **17**, 113108.

SAHAI, A., TSUNG, F., TABLEMAN, A., MORI W.B. & KATSOULEAS T.C. 2013 Relativistically induced transparency acceleration of light ions by an ultrashort laser pulse interacting with a heavy-ion-plasma density gradient. *Phys. Rev.* E **88**, 043105.

SANTALA, M., ZEPH, M., WATTS, I., BEG F.N., CLARK E., TATARAKIS M., KRUSHELNICK K., DANGOR A.E., MCCANNY T., SPENCER I., *et al.* 2000 Effect of the plasma density scale length on the direction of fast electrons in relativistic laser-solid interactions. *Phys. Rev. Lett* **84**, 1459–1462.

SAVIN, A., ROSS, A., ABOUSHELBAYA, R., MAYR M.W., SPIERS B., WANG R.H.-W. & NORREYS P.A. 2019 Energy absorption in the laser-qed regime. *Sci. Rep*. **9**, 8956.

SAVIN, A., ROSS, A., SERZANS, M., TRINES R.M.G.M., CEURVORST L., RATAN N., SPIERS B., BINGHAM R., ROBINSON A.P.L. & NORREYS P.A. 2017 Attosecond-scale absorption at extreme intensities. *Phys. Plasmas* **24**, 113103.

SCHWINGER, J. 1951 On gauge invariance and vacuum polarization. *Phys. Rev*. **82**, 664.

SHEN, B., LI, Y., YU, M.Y. & CARY, J. 2007 Bubble regime for ion acceleration in a laser-driven plasma. *Phys. Rev.* E **76**, 055402.

SILVA, L., MARTI, M., DAVIES, J., FONSECA R.A., REN C., TSUNG F.S. & MORI W.B. 2004 Proton shock acceleration in laser-plasma interactions. *Phys. Rev. Lett*. **92**, 015002.

SOKOLOV, I., NAUMOVA, N.M. & NEES, J. 2011 Numerical modeling of radiation-dominated and quantum-electrodynamically strong regimes of laser-plasma interaction. *Phys. Plasmas* **18**, 093109.

SOKOLOV, I., NEES, J.A., YANOVSKY, V., NAUMOVA N.M. & MOUROU G.A. 2010 Emission and its back-reaction accompanying electron motion in relativistically strong and qed-strong pulsed laser fields. *Phys. Rev.* E **81**, 036412.

SORBO, D.D., BLACKMAN, D., CAPDESSUS, R., SMALL K., SLADE-LOWTHER C., LUO W., DUFF M.J., ROBINSON A.P.L., MCKENNA P., SHENG Z.-M., *et al.* 2018 Efficient ion acceleration and dense electron–positron plasma creation in ultra-high intensity laser-solid interactions. *New J. Phys*. **20**, 033014.

STEINKE, S., VAN TILBORG, J., BENEDETTI, C., GEDDES C.G.R., SCHROEDER C.B., DANIELS J., SWANSON K.K., GONSALVES A.J., NAKAMURA K., MATLIS N.H., *et al.* 2016 Multi stage coupling of independent laser-plasma accelerators. *Nature* **530**, 190–193.

TAJIMA, T. & DAWSON, J. 1979 Laser electron accelerator. *Phys. Rev. Lett*. **43** (4), 267–270.

TAMBURINI, M., PEGORARO, F., PIAZZA, A.D., KEITEL C.H. & MACCHI A. 2010 Radiation reaction effects on radiation pressure acceleration. *New J. Phys*. **12**, 123005.

VSHIVKOV, V., NAUMOVA, N., PEGORARO, F. & BULANOV, S. 1998 Nonlinear electrodynamics of the interaction of ultra-intense laser pulses with a thin foil. *Phys. Plasmas* **5**, 2727.

WANG, W.-M., GIBBON, P., SHENG, M., LI, Y.-T. & ZHANG, J. 2017 Laser opacity in underdense preplasma of solid targets due to quantum electrodynamics effects. *Phys. Rev.* E **96**, 013201.

WILKS, S., KRUER, W., TABAK, M. & LANGDON A.B. 1992 Absorption of ultra-intense laser pulses. *Phys. Rev. Lett*. **69**, 1383.

WILKS, S., LANGDON, A., COWAN, T., ROTH M., SINGH M., HATCHETT S., KEY M.H., PENNINGTON D., MACKINNON A. & SNAVELY R.A. 2001 Ion acceleration by superintense laser-plasma interaction. *Phys. Plasmas* **8**, 542.

XU, Y., WANG, J., HORA, H., QI X., XING Y., YANG L. & ZHU W. 2018 Plasma block acceleration based upon the interaction between double targets and an ultra-intense linearly polarized laser pulse. *Phys. Plasmas* **25**, 043102.

YAZDANI, E., SADIGHI-BONABI, R., AFARIDEH, H., YAZDANPANAH J. & HORA H. 2014 Enhanced laser ion acceleration with a multi-layer foam target assembly. *Laser Particle Beams* **32**, 509–515.

YIN, L., ALBRIGHT, B., HEGELICH, B., BOWERS K.J., FLIPPO K.A., KWAN T.J.T. & FERNÁNDEZ J.C. 2007 Monoenergetic and Gev ion acceleration from the laser breakout afterburner using ultrathin targets. *Phys. Plasmas* **14**, 056706.

ZHANG, P., RIDGERS, C. & THOMAS, A. 2015 The effect of nonlinear quantum electrodynamics on relativistic transparency and laser absorption in ultra-relativistic plasmas. *New J. Phys*. **17**, 043051.

ZHANG, X., SHEN, B., JI, L., WANG F., WEN M., WANG W., XU J. & YU Y. 2010 Ultrahigh energy proton generation in sequential radiation pressure and bubble regime. *Phys. Plasmas* **17**, 123102.

https://doi.org/10.1017/S0022377821000982 Published online by Cambridge University Press